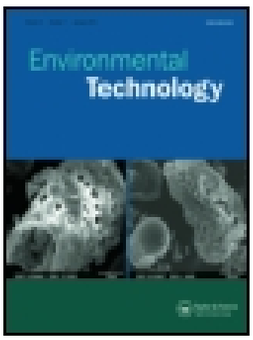

Environmental Technology

ISSN: 0959-3330 (Print) 1479-487X (Online) Journal homepage: http://www.tandfonline.com/loi/tent20

Characterization and phenol adsorption performance of activated carbon prepared from tea residue by NaOH activation

Jun Tao, Peili Huo, Zongheng Fu, Jin Zhang, Zhen Yang & Dengfeng Zhang

To cite this article: Jun Tao, Peili Huo, Zongheng Fu, Jin Zhang, Zhen Yang & Dengfeng Zhang (2017): Characterization and phenol adsorption performance of activated carbon prepared from tea residue by NaOH activation, Environmental Technology, DOI: 10.1080/09593330.2017.1384069

To link to this article: http://dx.doi.org/10.1080/09593330.2017.1384069

Accepted author version posted online: 22 Sep 2017.
Published online: 05 Oct 2017.

ENVIRONMENTAL TECHNOLOGY, 2017
https://doi.org/10.1080/09593330.2017.1384069

Taylor & Francis
Taylor & Francis Group

Characterization and phenol adsorption performance of activated carbon prepared from tea residue by NaOH activation

Jun Tao, Peili Huo, Zongheng Fu, Jin Zhang, Zhen Yang and Dengfeng Zhang

Faculty of Chemical Engineering, Kunming University of Science and Technology, Kunming, People's Republic of China

ABSTRACT

The preparation of activated carbon (AC) using tea residue was addressed in this work. The preparation process incorporated two-step pyrolysis and activation using NaOH. The influence of activation temperature between 500°C and 700°C on the properties of the AC sample was investigated. The physicochemical properties of the AC sample were characterized. The results show that the optimum temperature for the activation process is 700°C, which generates the AC sample with higher specific surface area and total pore volume, respectively, of 819 $m^2\ g^{-1}$ and 0.443 $cm^3\ g^{-1}$. The oxygen-containing functional groups evolve on the AC sample during the activation process. The phenol adsorption test was performed to evaluate the adsorption performance of the AC sample. The adsorption data confirm that phenol adsorption on the AC sample obtained at 700°C follows the pseudo-second-order kinetics model. Hereby, the electron donor–acceptor interaction mechanism can describe the adsorption process. The AC sample obtained at 700°C performs superior phenol adsorption performance. The maximum phenol adsorption capacity is 320 mg g^{-1}, which is higher than that of several AC samples reported previously. Thus, the tea residue acts as a good precursor for the AC with promising adsorption capacity by the NaOH chemical activation method.

ARTICLE HISTORY
Received 30 May 2017
Accepted 14 September 2017

KEYWORDS
Tea residue; activated carbon; two-step pyrolysis; adsorption; phenol removal

1. Introduction

The adsorption process is widely employed in both industrial and living fields. The selection of an appropriate adsorbent for a target adsorbate plays a dominant role in the adsorption process. The activated carbon (AC) has been extensively used as an adsorbent because of its well-developed pore morphology [1,2] and abundant functional groups [3,4]. However, the widespread usage of AC is restricted due to its higher manufacturing cost. Hitherto, the majority of carbonaceous materials such as coal and wood are always used as the precursors of the AC [5–7]. Nevertheless, carbonaceous waste, as an alternative precursor to prepare the AC, can significantly cut down the manufacturing cost [8]. The carbonaceous waste mainly consists of rice hull [9], nut shells [10], coffee grounds [11] and tobacco residues [12]. Numerous studies indicated that the carbonaceous wastes endow the AC with superior physicochemical properties [9,13,14].

As an important kind of carbonaceous waste, the tea residue is a potential candidate for the precursor of the AC [15–17]. The tea residue is derived from the tea consumption field. The tea, dried leaves of the *Camellia sinensis* species of theaceae family, is acknowledged as a popular beverage with a production of three million tons per year in China [18]. Many tons of the tea residue are generated during the consumption of the tea leaves. The preparation of the AC from the tea residue can not only produce the AC with low cost, but also realize the recycling application of the tea residue. Therefore, this work is performed to investigate the preparation method of the AC from the tea.

Hitherto, the activation procedure is always involved in the production of the AC. The activation method comprises chemical activation and physical activation [19]. Given the advantages of the lower activation temperature and the good adsorption performance of the prepared AC, chemical activation instead of physical activation is frequently adopted. The chemical activation is usually performed by a two-step pyrolysis process, i.e. carbonization step and chemical activation step. Specifically, the precursors are first carbonized at a temperature below 700°C to produce char. Then, the char is made to undergo the chemical activation process with the impregnation of chemical additive including potassium hydroxide (KOH) [20], sodium hydroxide (NaOH) [21], zinc chloride ($ZnCl_2$) [22] and phosphoric acid (H_3PO_4) [23,24] and followed by the

CONTACT Dengfeng Zhang dengfengz@aol.com Faculty of Chemical Engineering, Kunming University of Science and Technology, Kunming 650500, People's Republic of China

pyrolysis under a steam, carbon dioxide and nitrogen atmosphere.

Numerous studies focused on the phenol adsorption on the AC prepared from the tea residue using HNO_3 as the activating agent, and the obtained AC only performed with a lower adsorption capacity on phenol [25]. Thus, a novel and simple method to prepare the AC with superior adsorption performance was fully addressed in this study. Specifically, the AC sample was prepared through the simple two-step process. The effect of the activation temperature ranging between 500°C and 700°C on the physicochemical property of the prepared AC sample was studied. Finally, the phenol-containing waste water is an important representative of organic waste water due to its massive discharge and is a great threat to the ecosystem [8,26–28]. Thus, the phenol adsorption performance of the AC sample with well-developed pore morphology and surface oxygen-containing functional groups was also examined to demonstrate the feasibility of the AC sample obtained from this work used in the field of organic waste water treatment.

2. Experimental

2.1. Preparation procedures

The tea residue selected as the precursor of the AC was obtained from households. The detailed preparation procedures for the AC sample have been summarized as follows. The tea residue was ground and sieved to generate particles with grain diameter ≤ 0.35 mm. In the two-step process, the ground tea residue was pyrolyzed in a closed crucible to prepare carbonized products at 500°C. The carbonized products and sodium hydroxide (NaOH) were physically mixed at a mass ratio of 1:1 and milled for 0.5 h. The mixture was loaded in a closed crucible and chemically activated at 500°C, 600°C and 700°C and heated isothermally for 2 h. All of the aforementioned carbonization and activation procedures were conducted under the air atmosphere instead of the inert atmosphere or the oxidation atmosphere [17,29–31], which will decrease the preparation cost of the AC. After being cooled to room temperature, the obtained samples were thoroughly washed with distilled water until the pH of the final filtrate was around 7.0. Finally, the samples were filtered, dried and crushed in sequence. The generated samples with grain diameter between 0.074 and 0.15 mm were stored in a desiccator for the subsequent experiments. The AC samples produced at 500°C, 600°C and 700°C were designated as AC1, AC2 and AC3, respectively. The yield of each AC sample, defined as the percentage ratio of the weight of the AC sample to the weight of the tea residue used during the activation stage, was determined in this work. The results indicate that the yields of samples AC1, AC2 and AC3 are 33.12%, 28.58% and 25.33%, respectively, which further confirms that the yield decreases with the activation temperature.

2.2. Characterization methods

In this study, the methods including N_2 adsorption/desorption, scanning electron microscopy (SEM), X-ray diffraction (XRD) and X-ray photoelectron spectroscopy (XPS) were performed to determine the main physicochemical properties related to the adsorption performance of the AC samples.

The pore structure parameters of the AC samples, including pore size distributions, BET surface area and pore volume, were determined by low-temperature nitrogen adsorption/desorption at 77.4 K using a NOVA 4200e gas sorption analyzer provided by Quantachrome Corp., U.S.A. Prior to the analysis, all the samples were fully degassed under vacuum conditions for 12 h at 100°C. The specific surface area (S_{BET}) of each AC sample was calculated using the nitrogen adsorption data in the relative pressure (P/P_0) with a range of 0.05–0.30 according to the BET model [32]. The total pore volume (V_t) and the mesopore pore volume (V_{mes}) were determined using the nitrogen desorption data based on the BJH model [33]. The micropore area (S_{mic}) and volume (V_{mic}) were estimated by subtracting the mesopore area and V_{mes} from S_{BET} and V_t, respectively [34]. The average pore size (D_p) was determined from V_t and S_{BET} [35].

The images of the pore morphology of the AC samples were examined through SEM analysis operated on VEGA3-SBH, Tescan Corp., Czech. Prior to the SEM analysis, the AC samples were coated with a very thin layer of gold in a sputter-coater unit. The coated samples were analyzed at an accelerating voltage of 10 kV using a secondary electron detector.

To further investigate the crystallite structure of the AC samples, XRD analysis was conducted on a *D*/max-3B XRD spectrometer using Cu Kα radiation. The scanned angle (2θ) was limited between 10° and 90° with a step size of 10 min^{-1}. XPS analysis used to determine the chemical property of the AC samples was performed on an X-ray Photoelectron Spectrometer PHI 5000 VersaProbe-II supplied by ULVAC-PHI, Inc., Japan. The X-ray Photoelectron Spectrometer was equipped with an Al Ka X-ray source (1486.7 eV). The electron binding energies were calibrated based on the carbon (1s) peak at 284.8 eV [36].

2.3. Phenol adsorption test

Batch adsorption experiments were carried out by exposure of 1.00 g of the AC sample to 1000 mL of phenol-containing solution. The initial concentration of the phenol varied between 200 and 1400 mg L^{-1}. The adsorption process occurred in a flask, which was loaded in a thermostatic shaker bath at a rotating speed of 200 r min^{-1} and a temperature of 303 K. To analyze the phenol concentration during the adsorption process, the liquid sample was sampled by a finnpipette and filtered through 0.45 μm nitrocellulose membrane. Both the equilibrium concentration and the instantaneous concentration of phenol in the solution were measured by a PUXI T6 UV–VIS ultraviolet spectrophotometer. The analysis wavelength was set as 270 nm. Each test for the determination of the phenol concentration was carried out three times. The arithmetic mean value was designated to the final phenol concentration. The amount of phenol adsorption on the AC, designated as q_t, was calculated in mg g^{-1} by the following equation:

$$q_t = \frac{V(C_0 - C_t)}{m}, \quad (1)$$

where V (L) is the volume of the phenol-containing solution, C_0 (mg L^{-1}) is the initial phenol concentration, C_t (mg L^{-1}) is the instantaneous phenol concentration corresponding to t and m (g) is the dosage of the AC sample.

In order to improve the accuracy of the experimental adsorption data, a blank test using distilled water was carried out for each batch phenol adsorption experiment, and all the measured phenol adsorption data have been deducted the background data obtained from the blank test.

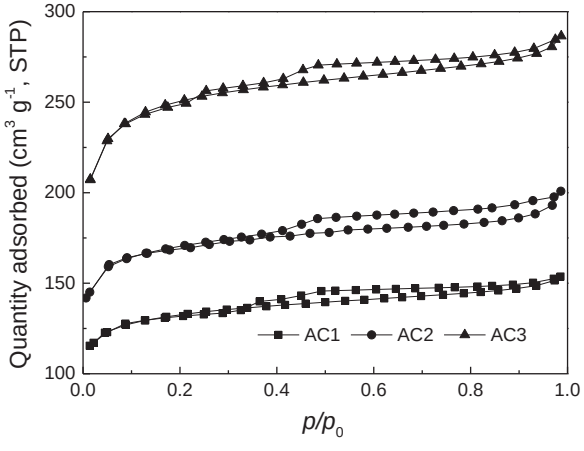

Figure 1. Nitrogen adsorption/desorption isotherms of all the AC samples at 77 K.

3. Results and discussion

3.1. Pore structure characteristics

The raw nitrogen adsorption/desorption isotherms and the pore structure parameters are shown in Figure 1 and Table 1, respectively. On the basis of the classification standard published by the International Union of Pure and Applied Chemistry (IUPAC) [37], the adsorption isotherms of all the AC samples, as shown in Figure 1, are found to follow the trend of the Type I isotherm. The Type I isotherm is always applicable to the adsorbent with abundant micropores. Table 1 indicates that both the pore area and the pore volume of the AC samples increase with the activation temperature. At a lower activation temperature, the organic matters release from the char and the carbon atoms react with NaOH partly. Thus, some micropores are developed. At a higher activation temperature, more carbon atoms are being consumed and more organic matters are released, which enhances the activation process and leads to the further creation of the pores [38,39].

The SEM images of the AC samples are displayed in Figure 2. Obvious differences between the surface morphology of the AC samples are observed from the images. As shown in Figure 2(a,d), the sample AC1 prepared with an activation temperature of 500°C exhibits a smoother pore surface and has only a small quantity of macropore entries or cracks. However, samples AC2 and AC3 (Figure 2(b,c,e,f)) present larger macropore entries or cracks, which are probably related to the more release of organic matters and the consumed carbon atoms during the chemical activation stage. Therefore, a higher activation temperature can create more macropore entries for adsorption and provide channels for phenol molecules to access the micropores and mesopores within the AC samples.

3.2. Crystallite structure characteristics

As shown in Figure 3, two broad peaks around 25° and 43° are found in the XRD profiles of all the AC samples, which are attributed to the disordered graphitic (002) and (100) planes, respectively. The wide peak (002) indicates the incomplete development of the micro-crystal structure, while the tiny peak (100) indicates that the disordered graphite layers are formed during the carbonization and activation process. The intensities of the peaks corresponding to (002) and (100) of samples AC1 and AC2 are stronger than that of sample AC3, and further suggests that the stacking structure of the layers is more ordered for both sample AC1 and sample AC2. The structure of sample AC3 appears disordered, which

Table 1. Pore structure parameters of all the AC samples.

Samples	S_{BET} ($m^2\ g^{-1}$)	S_{mic} ($m^2\ g^{-1}$)	S_{mes} ($m^2\ g^{-1}$)	V_{mic} ($cm^3\ g^{-1}$)	V_{mes} ($cm^3\ g^{-1}$)	D_p (nm)
AC1	429.45	251.59	177.86	0.151	0.086	1.136
AC2	567.22	270.58	296.64	0.163	0.152	1.144
AC3	819.63	290.00	529.63	0.216	0.227	1.149

accounts for its more developed pore structure. In addition, the XRD patterns of the AC samples display a small sharp diffraction peak around 29.4°, which is assigned to the crystal structure of $CaCO_3$. The formation of $CaCO_3$ is probably related to the composition of the precursor which contains a small proportion of Ca^{2+} [40]. The possible reactions between NaOH, C and Ca^{2+} are presented as follows:

$$-CH_2 + 4NaOH \rightarrow Na_2CO_3 + Na_2O + 3H_2, \quad (2)$$

$$Ca^{2+} + Na_2CO_3 \rightarrow CaCO_3 + 2Na^+. \quad (3)$$

3.3. Surface chemical property

In order to examine the surface functional groups induced by the NaOH activation method, XPS characterization was conducted for the obtained AC samples. The XPS spectra displayed in Figure 4 clearly show that the elements of C, O, N, Na, Ca and Mg are detected. The elemental compositions of C, O, N, Na, Ca and Mg of all the AC samples were determined from the integral peak area of each element and the sensitivity factors (0.31 for C, 0.73 for O, 0.49 for N, 1.1 for Na, 1.92 for Ca and 0.27 for Mg). The range of integration of each element is labeled in Figure 4.

Table 2 further presents the surface elemental composition for all the AC samples. Compared with sample AC1, the relative C contents on the surface of both sample AC2 and sample AC3 decrease while the relative surface oxygen contents exhibit an increasing trend. The aforementioned results also confirm that the more oxygen-containing functional groups are generated during the activation process operated at a higher temperature. In addition, N, Ca and Mg are also detected in all the AC samples prepared from the tea residue.

As shown in Figures 5 and 6, the XPS spectra of samples AC1, AC2 and AC3 present two distinct peaks, due to carbon (C 1s) and oxygen (O 1s). The deconvolution of C 1s spectra is decomposed into five peaks as listed in Table 3. The operation under a higher activation

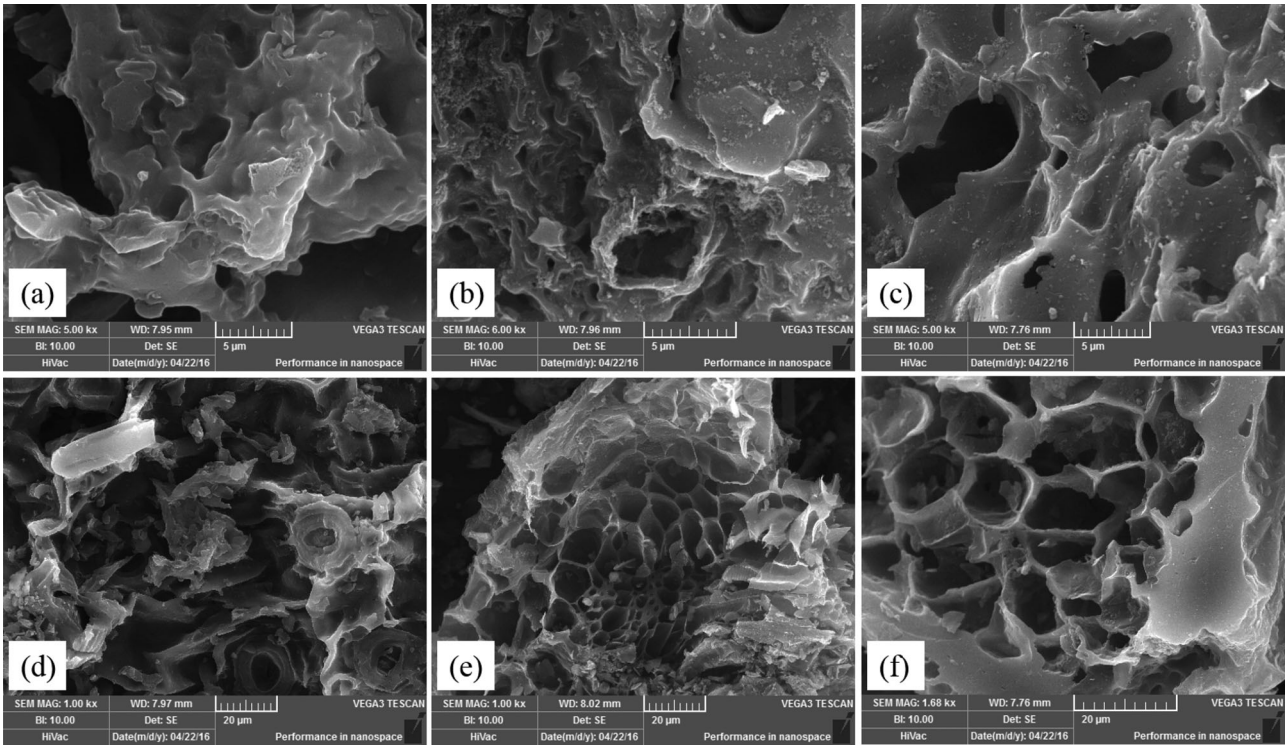

Figure 2. SEM images of all the AC samples: (a and d) AC1, (b and e) AC2 and (c and f) AC3.

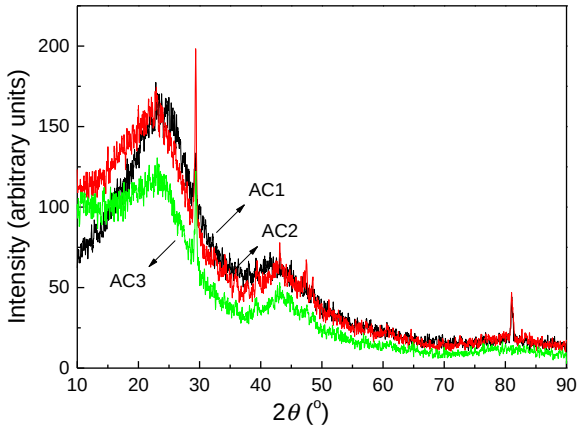

Figure 3. XRD patterns of all the AC samples.

temperature decreases the intensities of Peak C1, and increases the intensities of Peak C2, Peak C3 and Peak C4 assigned to the oxygen-containing functional groups. The increases in the surface concentrations of lactone, anhydride and carboxylic acid are mainly due to the higher activation temperature, whereas carbon in graphitic or aromatic surface structures significantly decreases as a result of the enhanced oxidation level. The XPS spectra of O 1s and the deconvolution results of the AC samples are shown in Figure 6 and Table 4, respectively. Three main peaks corresponding to carbonyl (Peak O1), carbonyl, hydroxyl, ester (Peak O2) and ether (Peak O3) are observed. The minor Peak O4 is assigned to a carboxyl group on the surface of the AC samples. Apparently, the intensities of Peak O2 are enhanced for the AC sample activated under a higher temperature; however, the intensities of Peak O3 tend to weaken significantly. The total amount of C=O groups (Peak O1) of samples AC1, AC2 and AC3 is high while that of the carboxyl group (Peak O4) is relatively weak. Such results

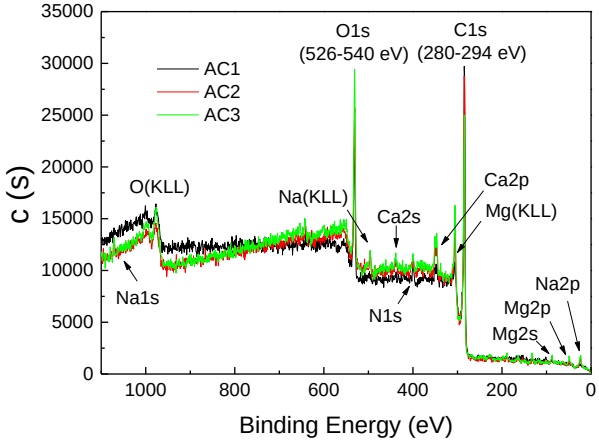

Figure 4. XPS spectra of all the AC samples.

Table 2. Surface composition of all the AC samples from the XPS spectra.

	Atomic concentration (%)					
Samples	C	O	N	Na	Ca	Mg
AC1	78.11	17.64	2.54	0.26	1.00	0.45
AC2	71.79	19.58	4.09	0.76	2.58	1.20
AC3	68.26	23.62	2.39	1.32	2.56	1.85

further confirm that the more carbonyl and hydroxyl groups are generated by NaOH activation at a higher activation temperature. Furthermore, the O/C atomic ratio of

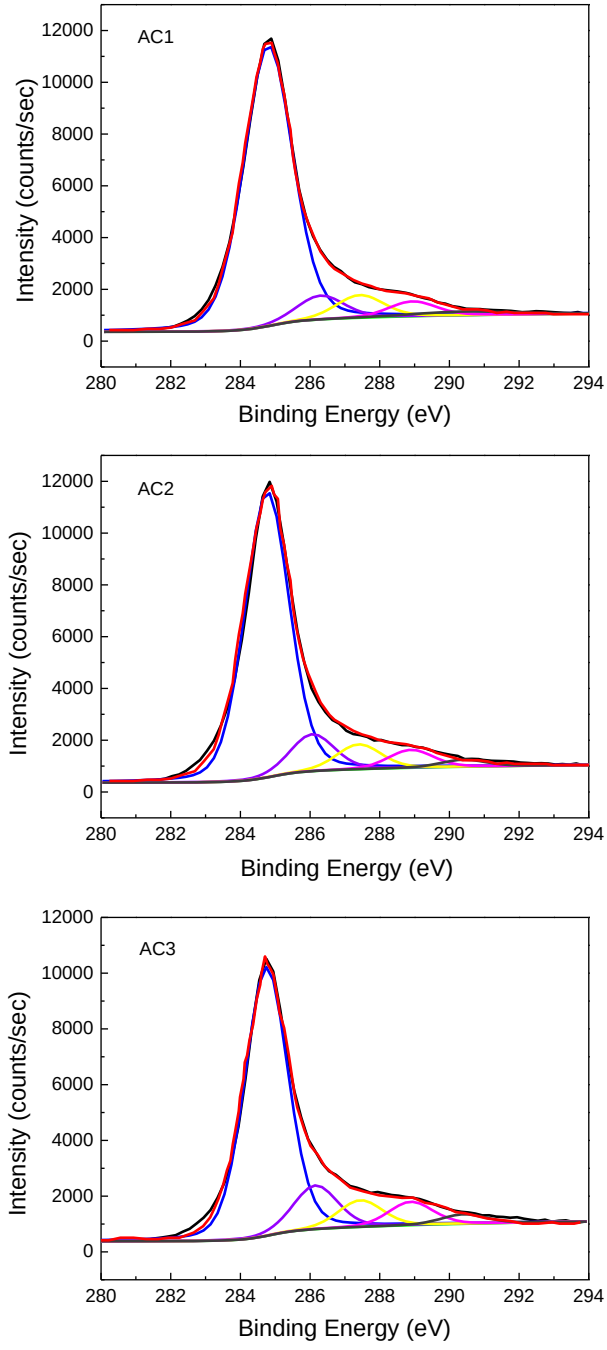

Figure 5. C 1s spectra calibrated according to the graphite C 1s peak at 284.8 eV of all the AC samples.

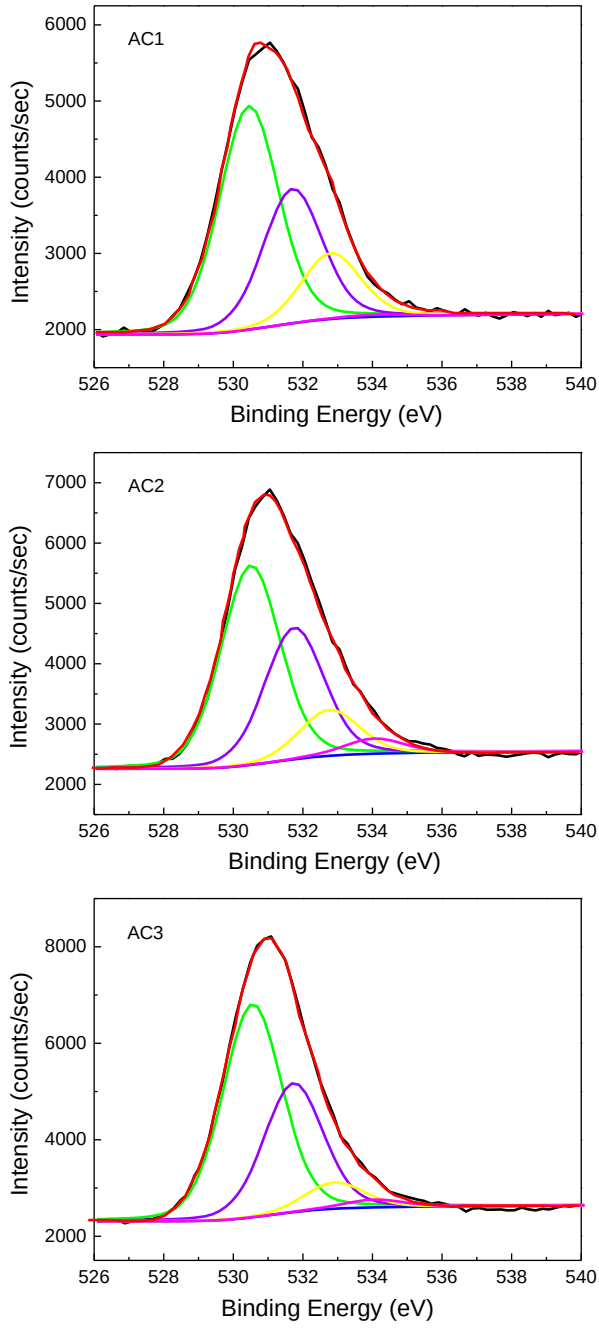

Figure 6. O 1s spectra calibrated according to the graphite C 1s peak at 284.8 eV of all the AC samples.

sample AC3 is greatly enhanced and indicates that the surface oxygen-containing species can be effectively created at a higher activation temperature.

3.4. Effect of activation temperature on phenol adsorption

The activation temperature dependence of phenol adsorption performance of the AC samples is illustrated in Figure 7. The increase in the activation temperature from 500°C to 700°C favors the phenol adsorption capacity of the AC samples. The pore morphology and the content of the functional group of an adsorbent are always dominant in an adsorption process [43,44]. On the one hand, the AC sample with well-developed pore structure has a stronger adsorption capability [45–47]. On the other hand, the main oxygen-containing functional groups also strongly affect the adsorption performance of the AC sample [48–50]. Specifically, the carbonyl groups promote phenol adsorption on the AC sample via the electron donor–acceptor interaction mechanism [51–53]. Thus, according to the pore structure parameters listed in Table 1, the sample AC3 is provided with larger pore area and pore volume. In addition, based on the deconvolution of the O 1s XPS profiles of all the AC samples listed in Table 4, the number of carbonyl groups of sample AC3 is more than samples AC1 and AC2. The aforementioned two aspects can account for the superior adsorption performance of phenol on sample AC3.

3.5. Kinetics study of phenol adsorption

The kinetics test of the phenol adsorption on sample AC3 with superior adsorption performance was also performed in this work. The effect of the initial phenol concentration on the adsorption capacity of sample AC3 is shown in Figure 8. A sharp increasing trend of phenol adsorption is observed during the initial 10 min. Subsequently, the adsorption rate decreases slightly and exhibits a plateau after approximately 60 min, which is probably due to the continuous reduction of active or open sites available for phenol adsorption during the adsorption process. As shown in Figure 9, the equilibrium adsorption amount (q_e) of phenol varies from 101 to 318 mg g^{-1} with the increase of phenol concentration from 200 to 1400 mg g^{-1}. The phenol adsorption capacity of sample AC3 is higher than that of the modified commercial AC and other biomass-based AC samples [4,54–56]. The relatively high adsorption

Table 3. Deconvolution of the C 1s XPS profiles of all the AC samples [41].

	Peak/binging energy (eV)				
Samples	Peak 1 (C1) 284.8 ± 0.1 Graphitic, aromatic or aliphatic carbon (%)	Peak 2 (C2) 286.2 ± 0.1 Ether or hydroxyl groups (%)	Peak 3 (C3) 287.5 ± 0.1 Carbonyl groups (%)	Peak 4 (C4) 288.9 ± 0.1 Carboxyl or ester groups (%)	Peak 5 (C5) 290.4 ± 0.1 π–π^* transitions in aromatic rings (%)
AC1	80.79	6.87	6.23	4.07	2.05
AC2	76.72	9.92	6.67	4.81	1.88
AC3	71.56	12.04	7.35	6.44	2.61

Table 4. Deconvolution of the O 1s XPS profiles of all the AC samples [42].

	Peak/binging energy (eV)				
Samples	Peak 1 (O1) 530.5 ± 0.1 O atoms in carbonyl groups (C=O) (%)	Peak 2 (O2) 531.7 ± 0.1 O atoms in hydroxyls, anhydrides, ether or esters (%)	Peak 3 (O3) 532.8 ± 0.1 O atoms in esters and anhydrides (%)	Peak 4 (O4) 534.1 ± 0.1 O atoms in carboxyl groups (%)	O/C (%)
AC1	52.51	31.58	15.47	0.44	22.6
AC2	50.88	33.54	11.75	3.83	27.3
AC3	56.69	34.28	6.99	2.05	34.6

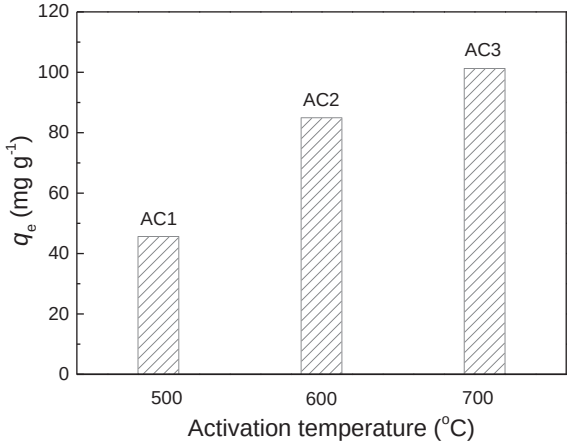

Figure 7. Effect of activation temperature on phenol capacity of all the AC samples.

capacity suggests that the sample AC3 possesses superior adsorption performance and potential application in the field of phenol-containing waste water treatment.

To provide further insight into the phenol adsorption kinetics behavior, the experimental data of the equilibrium adsorption capacity of phenol corresponding to the contact time were fitted with two adsorption kinetics models, i.e. the pseudo-first-order model and the pseudo-second-order model.

The original forms of the pseudo-first-order and the pseudo-second-order are given as:

$$\frac{dq_t}{dt} = k_1(q_{2e,\mathrm{cal}} - q_t), \tag{4}$$

$$\frac{dq_t}{dt} = k_2(q_{2e,cal} - q_t)^2. \tag{5}$$

The linear forms of the pseudo-first-order (Equation (6)) and the pseudo-second-order (Equation (7)) are expressed as follows:

$$\lg(q_{e,\exp} - q_t) = \lg q_{e,\mathrm{cal}} - \frac{k_1}{2.303}t, \tag{6}$$

$$\frac{t}{q_t} = \frac{1}{k_2 q_{e,\mathrm{cal}}^2} + \frac{t}{q_{e,\mathrm{cal}}}, \tag{7}$$

where k_1 (min^{-1}) and k_2 (g mg^{-1} min^{-1}) are the pseudo-first-order rate constant and pseudo-second-order rate constant, respectively, $q_{e,\exp}$ (mg g^{-1}) and $q_{e,\mathrm{cal}}$ (mg g^{-1}) are the amount of phenol adsorbed corresponding to the experimental-equilibrium state and the calculated-equilibrium state, respectively.

According to Equations (6) and (7), the items l g($q_{e,\exp} - q_t$) and t/q_t are assigned as the dependent variables, and t is assigned as the independent variable. Thus, the

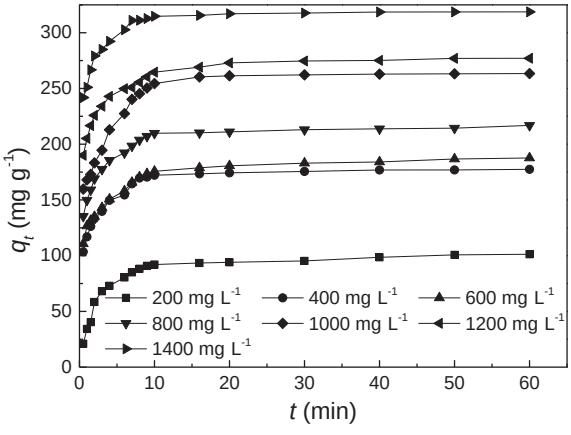

Figure 8. Effect of initial concentrations and contact time on the phenol adsorption amount.

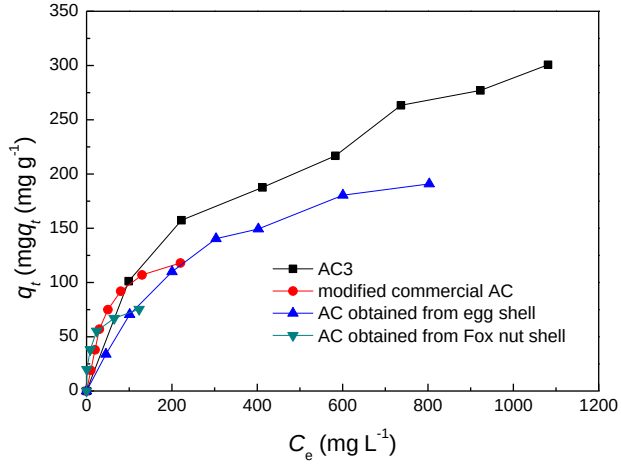

Figure 9. Comparison of phenol adsorption capacity with the AC samples reported in the previous works.

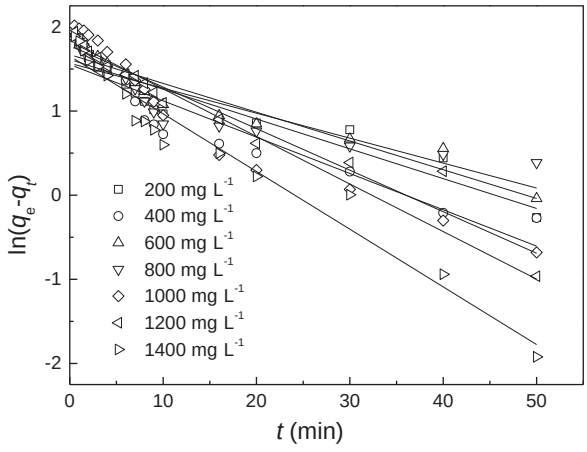

Figure 10. Plots of the pseudo-first-order kinetics models of phenol adsorption on sample AC3.

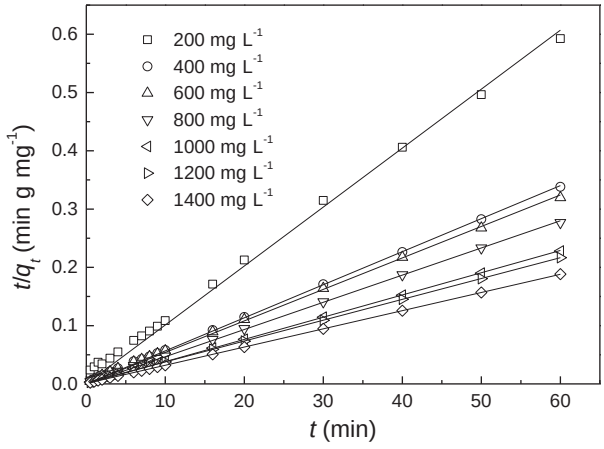

Figure 11. Plots of the pseudo-second-order kinetics models of phenol adsorption on sample AC3.

unknown parameters including $q_{e,cal}$, k_1 and k_2 can be obtained by the linear regression approach.

The fitting curves obtained from the pseudo-first-order model and the pseudo-second-order model are enclosed in Figures 10 and 11, respectively. The fitting parameters are summarized in Table 5. Both Figures 10 and 11 clearly show that the pseudo-second-order kinetics model fits the experimental profiles very well. As listed in Table 5, $q_{e,cal}$ is in good agreement with $q_{e,exp}$, and the multiple correlation coefficients (R^2) are higher than 0.9990 for different initial concentrations. The aforementioned results suggest that the pseudo-second-order kinetics model is more suitable to describe the experimental data than the pseudo-first-order kinetics model. According to the definition of the adsorption rate, d_q/d_t, the initial phenol adsorption rate at t = 0.5 min was used to determine the effect of the initial phenol concentration on the initial adsorption rate. As shown in Table 6, it is concluded that the initial adsorption rate increases with the elevated initial phenol concentration, which is related to the enhanced driving force of mass transfer at a higher phenol concentration. Several previous studies have reported the same results [4,57]. The superior fitting accuracy of the pseudo-second-order kinetics model suggests that the rate of the adsorption process is mainly controlled by chemisorption which involved valency changes through exchange or sharing of the electrons between the adsorbate and the adsorbent [58].

The oxygen-containing functional groups on the surface of the AC samples mainly comprise carboxyl, hydroxyl and carbonyl. It can be seen from Tables 3 and 4 that the quantities of carboxyl, hydroxyl and carbonyl groups on sample AC3 are higher than samples AC1 and AC2. The electron donor–acceptor mechanism incorporates the interaction of the carbonyl groups (electron donor) of the AC samples with the aromatic ring (electron acceptor) of the phenol [59]. It is acknowledged that the carbonyl groups promote phenol adsorption at the beginning of the adsorption experiment. However, once the carbonyl groups are exhausted, the electron donor–acceptor complexes cannot be formed [3]. It is observed that the phenol adsorption capacity sharply increases during the initial 10 min. The carboxyl and hydroxyl groups enhance the affinity of AC toward water and inhibit phenol adsorption by weakening the π–π dispersion interaction between the π electrons in the aromatic rings of the phenol molecule and the delocalized π electrons in the basal planes of the AC samples [60]. With regard to phenol adsorption, three mechanisms are widely accepted, i.e. the electron donor–

Table 5. Kinetics parameters for the adsorption of phenol with different initial concentrations on sample AC3.

		Pseudo-first-order kinetics model			Pseudo-second-order kinetics model		
Initial concentration (mg L^{-1})	$q_{e,exp}$ (mg g^{-1})	k_1 (min^{-1})	$q_{e,cal}$ (mg g^{-1})	R^2	k_2 (g mg^{-1} min^{-1})	$q_{e,cal}$ (mg g^{-1})	R^2
200	101.26	0.0816	41.12	0.8728	0.0055	103.69	0.9996
400	177.45	0.0994	35.72	0.8733	0.0091	179.31	0.9999
600	187.65	0.0787	46.83	0.9125	0.0063	189.35	0.9998
800	216.82	0.0683	36.93	0.7689	0.0080	217.71	0.9999
1000	263.35	0.1301	67.35	0.9251	0.0051	267.33	0.9998
1200	277.08	0.1137	60.07	0.9455	0.0065	279.49	0.9999
1400	318.68	0.1578	44.92	0.9551	0.0117	320.40	0.9999

Table 6. Initial adsorption rate corresponding to the initial phenol concentration.

Initial concentration (mg L^{-1})	200	400	600	800	1000	1200	1400
Initial adsorption rate (mg g^{-1} min^{-1})	41.98	206.86	221.33	270.67	319.42	380.01	483.63

acceptor interaction, dispersive interaction of π–π electron coupling and competing adsorption of solvent molecules [61]. Based on the aforementioned analyses, the electron donor–acceptor mechanism is more applicable for the adsorption of phenol on sample AC3.

4. Conclusions

This work presented an upgraded two-step pyrolysis method using tea residue as precursor to prepare AC. The results indicate that the optimum activation temperature is 700°C which can generate the AC sample, designated as sample AC3, with developed pore structure and abundant oxygen-containing functional groups. The specific surface area and total pore volume of sample AC3 are 819 m^2 g^{-1} and 0.443 cm^3 g^{-1}, respectively. The pseudo-second-order kinetics model can well describe phenol adsorption on sample AC3. The maximum phenol adsorption capacity of sample AC3 can reach 320 mg g^{-1}, which highlights its applicability for the organic compounds' removal from the waste water. The results prove that the preparation method of AC samples from tea residue by the two-step pyrolysis method has great success and potential, due to its shorter activation duration and lower manufacturing cost.

Disclosure statement

No potential conflict of interest was reported by the authors.

Funding

This work was supported by the Science Foundation of the Education Department of Yunnan Province [grant number 2015Y063], the Analysis and Measurement Foundation of Kunming University of Science and Technology [grant number 2016T20110217] and the National Natural Science Foundation of China [grant numbers 41762013 and 41302132].

ORCID

Dengfeng Zhang http://orcid.org/0000-0003-3102-7938

References

[1] Hameed BH, Rahman AA. Removal of phenol from aqueous solutions by adsorption onto activated carbon prepared from biomass material. J Hazard Mater. 2008;160:576–581.
[2] Caturla F, Martín-Martínez JM, Molina-Sabio M, et al. Adsorption of substituted phenols on activated carbon. J Colloid Interface Sci. 1988;124:528–534.
[3] Moreno-Castilla C. Adsorption of organic molecules from aqueous solutions on carbon materials. Carbon. 2004;42:83–94.
[4] Yang G, Chen HL, Qin HD, et al. Amination of activated carbon for enhancing phenol adsorption: effect of nitrogen-containing functional groups. Appl Surf Sci. 2014;293:299–305.
[5] Chen Y, Zhu YC, Wang ZC, et al. Application studies of activated carbon derived from rice husks produced by chemical-thermal process – a review. Adv Colloid Interface. 2011;163:39–52.
[6] Jibril BY, Al-Maamari RS, Hegde G, et al. Effects of feedstock pre-drying on carbonization of KOH-mixed bituminous coal in preparation of activated carbon. J Anal Appl Pyrol. 2007;80:277–282.
[7] Sahu JN, Acharya J, Meikap BC. Optimization of production conditions for activated carbons from tamarind wood by zinc chloride using response surface methodology. Bioresour Technol. 2010;101:1974–1982.
[8] Ahmaruzzaman M. Adsorption of phenolic compounds on low-cost adsorbents: a review. Adv Colloid Interface. 2008;143:48–67.
[9] Guo YP, Rockstraw DA. Activated carbons prepared from rice hull by one-step phosphoric acid activation. Microporous Mesoporous Mater. 2007;100:12–19.
[10] Savova D, Apak E, Ekinci E, et al. Biomass conversion to carbon adsorbents and gas. Biomass Bioenergy. 2001;21:133–142.
[11] Jung KW, Choi BH, Hwang MJ, et al. Fabrication of granular activated carbons derived from spent coffee grounds by entrapment in calcium alginate beads for adsorption of acid orange 7 and methylene blue. Bioresour Technol. 2016;219:185–195.
[12] Kilic M, Apaydin-Varol E, Pütün AE. Adsorptive removal of phenol from aqueous solutions on activated carbon prepared from tobacco residues: equilibrium, kinetics and thermodynamics. J Hazard Mater. 2011;189:397–403.
[13] Li SJ, Han KH, Li JX, et al. Preparation and characterization of super activated carbon produced from gulfweed by KOH activation. Micropor Mesopor Mater. 2017;243:291–300.
[14] Ahmad AA, Hameed BH. Effect of preparation conditions of activated carbon from bamboo waste for real textile wastewater. J Hazard Mater. 2010;173:487–493.
[15] Islam MA, Benhouria A, Asif M, et al. Methylene blue adsorption on factory-rejected tea activated carbon prepared by conjunction of hydrothermal carbonization and sodium hydroxide activation processes. J Taiwan Inst Chem Eng. 2015;52:57–64.
[16] Gundogdu A, Duran C, Senturk HB, et al. Physicochemical characteristics of a novel activated carbon produced from tea industry waste. J Anal Appl Pyrol. 2013;104:249–259.

[17] Kan YJ, Yue QY, Li D, et al. Preparation and characterization of activated carbons from waste tea by H_3PO_4 activation in different atmospheres for oxytetracycline removal. J Taiwan Inst Chem Eng. 2017;71:494–500.
[18] Peng C, Yan XB, Wang RT, et al. Promising activated carbons derived from waste tea-leaves and their application in high performance supercapacitors electrodes. Electrochim Acta. 2013;87:401–408.
[19] Cagnon B, Py X, Guillot A, et al. Contributions of hemicellulose, cellulose and lignin to the mass and the porous properties of chars and steam activated carbons from various lignocellulosic precursors. Bioresour Technol. 2009;100:292–298.
[20] Illán-Gómez MJ, García-García A, Salinas-Martínez de Lecea C, et al. Activated carbons from Spanish coals. 2. Chemical activation. Energy Fuels. 1996;10:1108–1114.
[21] Lin L, Zhai SR, Xiao ZY, et al. Dye adsorption of mesoporous activated carbons produced from NaOH-pretreated rice husks. Bioresour Technol. 2013;136:437–443.
[22] Hsu LY, Teng H. Influence of different chemical reagents on the preparation of activated carbons from bituminous coal. Fuel Process Technol. 2000;64:155–166.
[23] Diao YL, Walawender WP, Fan LT. Activated carbons prepared from phosphoric acid activation of grain sorghum. Bioresour Technol. 2002;81:45–52.
[24] Li KQ, Zheng Z, Li Y. Characterization and lead adsorption properties of activated carbons prepared from cotton stalk by one-step H_3PO_4 activation. J Hazard Mater. 2010;181:440–447.
[25] Gokce Y, Aktas Z. Nitric acid modification of activated carbon produced from waste tea and adsorption of methylene blue and phenol. Appl Surf Sci. 2014;313:352–359.
[26] Schobert HH, Song C. Chemicals and materials from coal in the 21st century. Fuel. 2002;81:15–32.
[27] Calace N, Nardi E, Petronio BM, et al. Adsorption of phenols by papermill sludges. Environ Pollut. 2002;118:315–319.
[28] Soni U, Bajpai J, Singh SK, et al. Evaluation of chitosan-carbon based biocomposite for efficient removal of phenols from aqueous solutions. J Water Process Eng. 2017;16:56–63.
[29] Prauchner MJ, Rodríguez-Reinoso F. Preparation of granular activated carbons for adsorption of natural gas. Micropor Mesopor Mater. 2008;109:581–584.
[30] Puziy AM, Poddubnaya OI, Martínez-Alonso A, et al. Oxygen and phosphorus enriched carbons from lignocellulosic material. Carbon. 2007;45:1941–1950.
[31] de Yuso AM, Rubio B, Izquierdo MT. Influence of activation atmosphere used in the chemical activation of almond shell on the characteristics and adsorption performance of activated carbons. Fuel Process Technol. 2014;119:74–80.
[32] Brunauer S, Emmett PH, Teller E. Adsorption of gases in multimolecular layers. J Am Chem Soc. 1938;60:309–319.
[33] Barrett EP, Joyner LG, Halenda PP. The determination of pore volume and area distributions in porous substances. 1. Computations from nitrogen isotherms. J Am Chem Soc. 1951;73:373–380.
[34] Gurten II, Ozmak M, Yagmur E, et al. Preparation and characterisation of activated carbon from waste tea using K_2CO_3. Biomass Bioenergy. 2012;37:73–81.
[35] Zhang DF, Zhang J, Huo PL, et al. Influences of SO_2, NO, and CO_2 exposure on pore morphology of various rank coals: implications for coal-fired flue gas sequestration in deep coal seams. Energy Fuels. 2016;30:5911–5921.
[36] Zhang DF, Wang HH, Wang QQ, et al. Interactions of nitric oxide with various rank coals: implications for oxy-coal combustion flue gas sequestration in deep coal seams with enhanced coalbed methane recovery. Fuel. 2016;182:704–712.
[37] Alcañiz-Monge J, Cazorla-Amorós D, Linares-Solano A, et al. Effect of the activating gas on tensile strength and pore structure of pitch-based carbon fibres. Carbon. 1994;32:1277–1283.
[38] Muniandy L, Adam F, Mohamed AR, et al. The synthesis and characterization of high purity mixed microporous/mesoporous activated carbon from rice husk using chemical activation with NaOH and KOH. Micropor Mesopor Mater. 2014;197:316–323.
[39] Wu MB, Li RC, He XJ, et al. Microwave-assisted preparation of peanut shell-based activated carbons and their use in electrochemical capacitors. New Carbon Mater. 2015;30:86–91.
[40] Aguayo-Villarreal IA, Bonilla-Petriciolet A, Muñiz-Valencia R. Preparation of activated carbons from pecan nutshell and their application in the antagonistic adsorption of heavy metal ions. J Mol Liq. 2017;230:686–695.
[41] Zielke U, Hüttinger KJ, Hoffman WP. Surface-oxidized carbon fibers. I. Surface structure and chemistry. Carbon. 1996;34:983–998.
[42] Figueiredo JL, Pereira MFR, Freitas MMA, et al. Modification of the surface chemistry of activated carbons. Carbon. 1999;37:1379–1389.
[43] Li L, Quinlivan PA, Knappe DRU. Effects of activated carbon surface chemistry and pore structure on the adsorption of organic contaminants from aqueous solution. Carbon. 2002;40:2085–2100.
[44] Alam MZ, Ameem ES, Muyibi SA, et al. The factors affecting the performance of activated carbon prepared from oil palm empty fruit bunches for adsorption of phenol. Chem Eng J. 2009;155:191–198.
[45] Dural MU, Cavas L, Papageorgiou SK, et al. Methylene blue adsorption on activated carbon prepared from *Posidonia oceanica* (L.) dead leaves: kinetics and equilibrium studies. Chem Eng J. 2011;168:77–85.
[46] Cazetta AL, Vargas AMM, Nogami EM, et al. NaOH-activated carbon of high surface area produced from coconut shell: kinetics and equilibrium studies from the methylene blue adsorption. Chem Eng J. 2011;174:117–125.
[47] Nowicki P, Kazmierczak-Razna J, Pietrzak R. Physicochemical and adsorption properties of carbonaceous sorbents prepared by activation of tropical fruit skins with potassium carbonate. Mater Design. 2016;90:579–585.
[48] Deng LL, Lu BQ, Li JL, et al. Effect of pore structure and oxygen-containing groups on adsorption of dibenzothiophene over activated carbon. Fuel. 2017;200:54–61.
[49] Bian Y, Bian ZY, Zhang JX, et al. Adsorption of cadmium ions from aqueous solutions by activated carbon with oxygen-containing functional groups. Chin J Chem Eng. 2015;23:1705–1711.
[50] Wang YB, Su XL, Xu Z, et al. Preparation of surface-functionalized porous clay heterostructures via carbonization of soft-template and their adsorption performance for toluene. Appl Surf Sci. 2016;363:113–121.
[51] Cheng WP, Gao W, Cui XY, et al. Phenol adsorption equilibrium and kinetics on zeolite X/activated carbon composite. J Taiwan Inst Chem Eng. 2016;62:192–198.

[52] Lorenc-Grabowska E, Gryglewicz G, Diez MA. Kinetics and equilibrium study of phenol adsorption on nitrogen-enriched activated carbons. Fuel. 2013;114:235–243.
[53] Lahaye J. The chemistry of carbon surfaces. Fuel. 1998;77:543–547.
[54] Zhang DF, Huo PL, Liu W. Behavior of phenol adsorption on thermal modified activated carbon. Chin J Chem Eng. 2016;24:446–452.
[55] Giraldo L, Moreno-Piraján JC. Study of adsorption of phenol on activated carbons obtained from eggshells. J Anal Appl Pyrol. 2014;106:41–47.
[56] Kumar A, Jena HM. Removal of methylene blue and phenol onto prepared activated carbon from Fox nutshell by chemical activation in batch and fixed-bed column. J Clean Prod. 2016;137:1246–1259.
[57] Mohanty K, Das D, Biswas MN. Adsorption of phenol from aqueous solutions using activated carbons prepared from *Tectona grandis* sawdust by $ZnCl_2$ activation. Chem Eng J. 2005;115:121–131.
[58] Hameed BH. Spent tea leaves: a new non-conventional and low-cost adsorbent for removal of basic dye from aqueous solutions. J Hazard Mater. 2009;161:753–759.
[59] Mattson JA, Mark HB, Malbin MD, et al. Surface chemistry of active carbon: specific adsorption of phenols. J Colloid Interface Sci. 1969;31:116–130.
[60] Coughlin RW, Ezra FS. Role of surface acidity in the adsorption of organic pollutants on the surface of carbon. Environ Sci Technol. 1968;2:291–297.
[61] Terzyk AP. Further insights into the role of carbon surface functionalities in the mechanism of phenol adsorption. J Colloid Interface Sci. 2003;268:301–329.